environments

MDPI

Article

Effect of Xanthan Gum on Soil Cracking in the Process of Water Reduction

Binbin Yang [1,2] and Yidan Yin [3,*]

[1] School of Civil Engineering, Xuchang University, Xuchang 461000, China; yangbinbin@xcu.edu.cn
[2] School of Civil Engineering, Wuhan University, No. 299 Bayi Road, Wuhan 430072, China
[3] School of Civil and Transportation Engineering, Beijing University of Civil Engineering and Architecture, Beijing 102616, China
* Correspondence: 1108140025036@stu.bucea.edu.cn

Abstract

Soil degradation is caused by frequent extreme weather events. The acceleration of soil degradation is due to the development of soil fissures, which form additional channels for water evaporation. This article investigates the effects of different concentrations of xanthan gum on soil water retention and crack resistance. The results indicate that xanthan gum slows down soil cracking and effectively enhances soil crack resistance. This article defines the first batch of cracks that appear at the beginning of crack formation as "trunks", cracks branching from the trunks as "branches", and cracks splitting from the branches as "twigs". As the content of xanthan gum increases, the trunks decrease and gradually turn into branches and twigs. Compared with soil with a xanthan gum content of 0.2%, the fractal dimension and fracture rate of soil samples decreased by 8.62%, 26.83%, and 35.45% and 2.75%, 13.74%, and 20.88%, respectively, when the xanthan content was 0.4%, 0.6%, and 0.8%. The final residual water content of the soil increased by 30%, 142%, and 192.5%, respectively. Compared with soil with a xanthan gum content of 0.8%, soil with a xanthan gum concentration of 0.2% showed a 150% increase in deceleration phase time. Xanthan gum affects the evaporation process and fracture behavior by altering the pore volume of the soil and generating biological aggregates. This study provides new ideas for the use of xanthan gum in solving soil cracking caused by dryness and water-retention problems.

Keywords: soil degradation; semi-arid regions; soil desiccation cracking; xanthan gum

1. Introduction

Soil, as the foundation of construction projects, has a negative impact on the safety of engineering construction when it develops cracks caused by dryness and cracking. As shown in Figure 1, soil drought cracking is a regional phenomenon. Soil drying and cracking, which is mainly caused by the tensile stress generated by the soil during the evaporation and drying process exceeding the tensile strength of the soil itself, is a very common manifestation [1–3]. The cracks generated by drying and cracking have a negative impact on the characteristics of soil. The presence of cracks exposes the surface soil and enhances the infiltration effect of rainfall, creating preferential flow paths for rainfall and pollutants, thereby affecting soil hydrological processes [4–7]. The appearance of soil cracks has a serious impact on the mechanical properties of upper structures, slopes, and foundations. Cracks weaken the stability and shear strength of soil structures and increase the compressibility of soil [8–10]. In agriculture, soil cracking has an impact on the

Check for updates

Academic Editor: Joaquim Esteves Da Silva

Received: 4 February 2026
Revised: 27 May 2026
Accepted: 29 May 2026
Published: 2 June 2026

Copyright: © 2026 by the authors. Licensee MDPI, Basel, Switzerland. This article is an open access article distributed under the terms and conditions of the Creative Commons Attribution (CC BY) license.

growth performance of plant roots, causing the breakage of existing roots and limiting the development of growing roots, ultimately resulting in soil nutrient loss [11]. Studying soil evaporation cracking behavior is crucial for enhancing soil drought resistance.

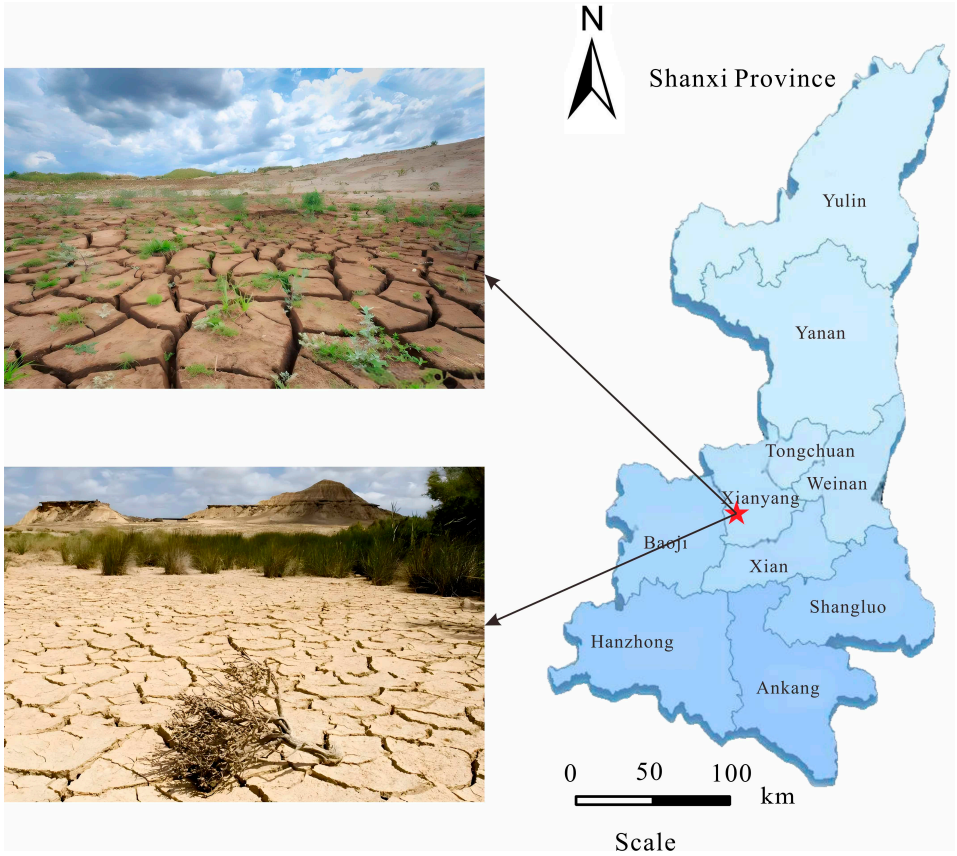


Figure 1. Drought status in the Shaanxi Region.

Researchers have conducted numerous experiments in the laboratory and in situ to investigate the factors and mechanisms of soil evaporation and soil drying cracking [12–14]. However, a critical comparison of recent studies reveals that as soil loses moisture, the disruption of capillary continuity and the alteration of vapor diffusion pathways fundamentally govern the drying process. Experiments have shown that soil evaporation and soil drying cracking interact with each other. Soil evaporation leads to soil drying cracking, while soil cracking also promotes further soil evaporation [15]. This dynamic hydro-physical state directly drives the mechanical response: soil evaporation leads to moisture loss, and the increasing matrix suction generates shrinkage-induced tensile stress. The impact of soil cracking on evaporation depends on the width and number of cracks [16]. The internal factor of soil cracking is due to the evaporation of soil moisture, which increases the tensile stress and suction force of the soil, exceeding the soil's tolerable state and resulting in cracks [1]. However, a key methodological limitation in prior work is that external factors (such as temperature, moisture content, and soil microstructure [17,18]) are typically evaluated in isolation. Without a critical synthesis of these interacting variables, the cracking process is rarely analyzed as a fully coupled hydro–mechanical system. This gap highlights an ongoing scholarly debate regarding how specific amendments interact with these underlying micro-physical mechanisms.

In recent years, researchers have chosen appropriate soil additives to improve soil water retention and reduce soil cracking. However, some traditional soil improvement materials, such as cement and lime, may lead to environmental concerns due to carbon emissions and potential soil contamination. In addition, materials such as biochar and

fibers also impact environmental conditions, although they are effective in improving water retention and reducing cracking., also impact the environmental conditions. Therefore, there is a need to explore more efficient and environmentally friendly alternatives. Biopolymers, as naturally occurring polymers, have attracted widespread attention with the increasing public awareness of the need for environmental protection. Xanthan gum is a biopolymer with excellent physicochemical properties, including high water absorption capacity, strong viscosity, and the ability to form stable hydrogel networks. It contains abundant hydroxyl and carboxyl functional groups, which enable strong interactions with soil particles through hydrogen bonding and electrostatic attraction. These properties allow xanthan gum to effectively bind soil particles, reduce pore connectivity, and improve water retention, making it a promising material for soil improvement. Due to its advantages of sustainability, environmental friendliness, and biodegradability [19,20], it is widely used as a soil amendment [21,22]. When the biopolymer encounters water, it will form a gel-like grid, filling the pore space of the soil, thus impeding the permeability of water [23]. It can also act as a binder to join soil particles and improve soil structure [24,25]. Biopolymer β-1,3/1,6-glucan has been shown to aggregate soil particles, thereby improving the overall compressive strength of soil. The same biopolymer has a positive impact on the compaction, Atterberg limit, and swelling index of treated soil but a negative impact on the consolidation coefficient [26]. The presence of biopolymers has an inhibitory effect on sediment loss caused by erosion and can enhance the cohesion between soil particles [27]. Alginate-based composite materials are believed to improve soil fertility and promote crop growth [28]. Xanthan gum, as an easily obtainable biopolymer material, has become one of the most widely used adhesives due to its low cost and high yield. Xanthan gum is more effective in improving tensile strength compared to pectin and alginate [29] and can effectively increase the fatigue life or bearing capacity of soil; thus, it can be used to improve the mechanical behavior of soil [30].

Although xanthan gum has been extensively studied as a soil stabilizer, previous research has primarily focused on its effects on improving soil mechanical properties and strength. However, the coupling relationship between evaporation dynamics and crack development in soils treated with different xanthan gum contents has received relatively little attention. To address this deficiency, the conceptual framework of this study incorporates the well-established desiccation mechanism. In this sequential process, evaporation drives water loss and increases internal matrix suction. This induces volumetric soil shrinkage and tensile stress accumulation, which ultimately drive crack propagation. Building upon this theoretical background, this study explores how varying xanthan gum concentrations modify the overall cracking behavior.

Therefore, this study aims to systematically investigate the impact of xanthan gum on soil water retention capacity and the extent of crack propagation on soils treated with four different xanthan gum concentrations through laboratory desiccation experiments and image analysis techniques. The quantitative characterization of crack networks is crucial for evaluating the inhibitory effect of xanthan gum on soil cracking. Furthermore, by quantifying the relationship between xanthan gum content and soil evaporation stages, this paper proposes a hierarchical crack classification framework (“trunk–branch–twig”) to describe the crack evolution process. This study provides new insights into the application of biopolymers for mitigating soil-desiccation cracking. Reducing these cracks through xanthan gum treatment has profound practical significance for enhancing mechanical stability and improving water conservation in engineering practices.

2. Materials and Methods

2.1. Materials

The soil used in this experiment was taken from Xianyang City, Shaanxi Province, China, with geographical coordinates N: N34°29′26″ and E: 108°45′41″. The area is located in a continental monsoon climate zone, with distinct hot, cold, dry, and wet seasons. In spring, water vapor is relatively scarce, cold air occasionally invades, and there are often strong winds and sandstorms. The highest precipitation received is only 41.7 mm. The extreme maximum temperature in summer can reach 42 °C, with an average precipitation of 141.17 mm, making it hot and rainy. The annual average temperature is around 10 °C, and the annual precipitation is 544.7 mm. The region supports developed agriculture, with the main crops being wheat, corn, and soybeans. However, due to its location in the Central Plains, the problem of drought is very severe. The serious problem of soil degradation in this region is due to the frequent evaporation of soil moisture caused by long-term lack of rainfall and persistent hot weather.

After on-site soil sampling, the specimen is air dried, crushed, and sieved through a 2 mm sieve. Subsequently, its basic physical properties are determined, as shown in Table 1 and Figure 2. All physical property tests were conducted in triplicate, and the reported values represent the average of three measurements, with corresponding variations within acceptable experimental error. Based on the Unified Soil Classification System (USCS), the measured liquid limit (29.6%), and the plasticity index (11.3%), the soil is classified as low-plasticity clay (CL).

Table 1. Basic physical properties of the soil samples.

Natural Water Content /%	Dry Density /g·cm^{-3}	Optimum Moisture Content /%	Maximum Dry Density /g·cm^{-3}	Liquid Limit %	Plastic Limit/%	Liquidity Index%	Plasticity Index %
14.9	1.59	17.5	1.7	29.6	18.6	−0.3	11.3



Figure 2. Illustration of soil cracking and its impacts: simplified diagram of cracked soil structure (soil particles, air, and water) and the impacts on agricultural systems, infrastructure, and buildings.

To measure the particle size, a Bettersize 2600 laser particle size analyzer (Dandong Bettersize Instruments Ltd., Dandong, China) was used. As shown in Figure 3, loess is mainly composed of silt and clay particles, with silt accounting for 72.28% and clay

accounting for 24.32%. Since the uniformity coefficient of loess is Cu = 4.45 and the curvature coefficient is Cc = 1, the grading of loess is poor.

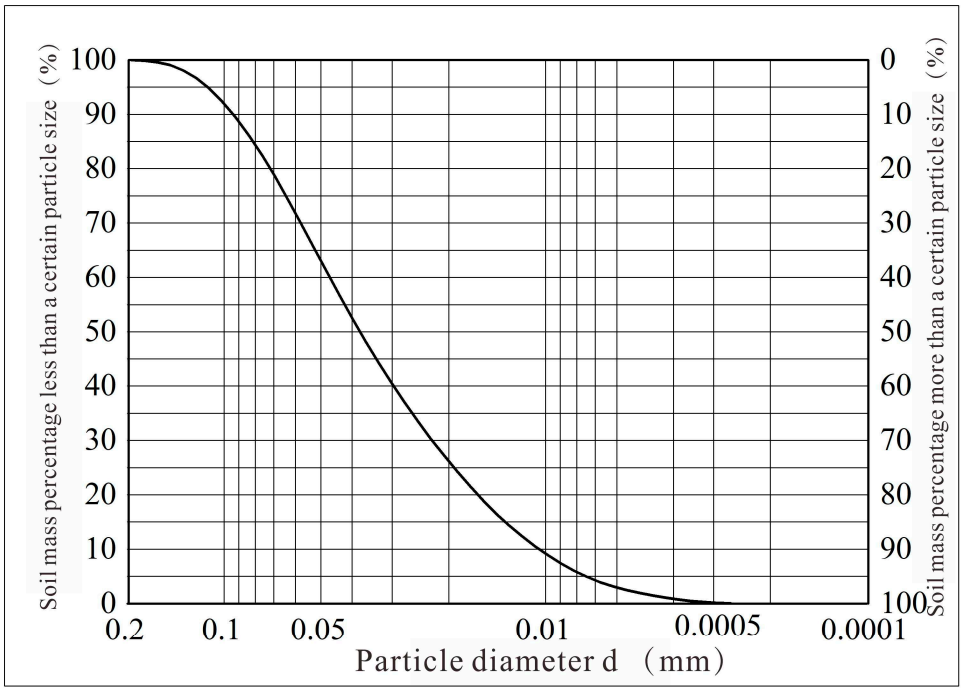


Figure 3. Grain-size distribution curve of the loess.

The solid form of xanthan gum is a white powder. When mixed with water, it can form a stable viscous gel, even at low concentrations [31]. When xanthan gum is used in soil, it provides bonds between soil particles and can serve as a soil enhancer [32]. It has excellent cold water solubility, pH stability, storage stability, ion salt compatibility, and pseudoplastic flow characteristics [33,34]. Due to the environmental friendliness and aforementioned characteristics of xanthan gum, it is expected to be used as an organic additive in bio-geotechnical engineering. Xanthan gum, as a type of biopolymer, is mainly obtained from corn starch and other raw materials through biological fermentation engineering cultivation, ethanol extraction, drying, and crushing. It is an extracellular acidic heteropolysaccharide produced by fermentation of Xanthomonas campestris.

When making xanthan gum, mix corn starch with water in a 1:4 ratio to form a suspension, and then heat it until it becomes a paste. Mix 2.5% gelatinized corn starch with a 0.3% nitrogen source (soybean flour, yeast extract, etc.), minerals (phosphate, magnesium powder, etc.), and other nutrients to form a complete fermentation medium, and adjust the pH value to 6.5. Sterilize the culture medium at a temperature greater than 120 °C to ensure that it is free of impurities. The activated strains of Xanthomonas campestris are cultured in primary and secondary stages in seed fermentation tanks. Inoculate the cultured bacterial solution into the production fermentation tank at a ratio of 5–10% to start the large-scale fermentation production of xanthan gum. Fermentation usually takes 2–4 days. During this process, the temperature needs to be maintained at 30 °C, the pH needs to be maintained at 6.5, and the supply of oxygen needs to be ensured. After fermentation, filter out the bacterial cells and leave behind the fermentation broth. Then add ethanol to extract collagen and filter again to obtain the xanthan gum precipitate. The xanthan gum precipitate will be washed, precipitated, dried, crushed, and sieved to obtain xanthan gum powder. The xanthan gum used in this study was commercially obtained from Otheredu, Henan, China, with a reported purity of ≥99%. The material complies with standard specifications for xanthan gum and exhibits typical physicochemical properties, including high molecular

weight polysaccharide structure, excellent water solubility, and pseudoplastic rheological behavior. These characteristics are consistent with those reported in previous studies, confirming the reliability of the material used in this study.

2.2. Experiments

The selected xanthan gum contents (0.2%, 0.4%, 0.6%, and 0.8%) were determined based on previous studies indicating that effective biopolymer stabilization typically occurs within the range of 0.1–1.0%. It should be explicitly emphasized that the primary objective of this experimental design is to investigate the effect of varying xanthan gum contents on cracking behavior rather than on the binary effect of its presence versus absence. The fundamental effectiveness of xanthan gum-treated compared to untreated soil (0%) has already been extensively validated in the existing literature. Therefore, to tightly focus on the concentration-dependent mechanisms and identify optimal dosage thresholds, this study deliberately utilizes the 0.2% treatment as the functional baseline to evaluate the evolutionary kinetics of higher concentrations (up to 0.8%). Concentrations lower than 0.2% may be insufficient to provide adequate bonding effects, whereas higher concentrations may lead to excessive pore blockage and reduced soil workability. The xanthan gum content was defined as the mass ratio of xanthan gum to dry soil, following the conventional definition commonly adopted in biopolymer-treated soil studies. Accordingly, the required xanthan gum dosage was calculated based on the dry mass of soil using Equation (1).

A slurry sample with a moisture content of 100% was prepared from the mixture. As a widely adopted standard procedure in soil desiccation cracking studies, this initially saturated state (well above the liquid limit) was deliberately chosen to erase the previous stress history of the soil and ensure a completely homogeneous initial matrix. The amount of added water was determined based on the target moisture content of the soil sample, taking into account the initial water content of the air-dried soil. This calculation follows the standard moisture adjustment method widely used in soil preparation procedures and is expressed in Equation (2).

The prepared mud sample is placed in a circular glass container with a diameter of 18 cm and a height of 2.5 cm. The shallow depth minimizes vertical moisture gradients to focus on 2D surface evaporation. While any finite container introduces inevitable boundary effects, a circular axisymmetric boundary specifically prevents artificial stress concentration at the corners (common in square molds), allowing for a natural radial crack evolution. The sample is vibrated using a vibration table for 5 min to eliminate any air bubbles inside the mud sample. To ensure statistical rigor and reproducibility, the evaporation and desiccation cracking experiments for each of the four xanthan gum concentrations (0.2%, 0.4%, 0.6%, and 0.8%) were conducted in triplicate (n = 3), resulting in a total of 12 independent samples. The reported data for dynamic parameters, including evaporation rates, crack ratios, and fractal dimensions, represent the average values derived from these three parallel replicate tests, ensuring that the variations fall within acceptable experimental error. It is important to acknowledge that the current laboratory setup (25 °C, 20% RH) represents a simplified, extreme drying event. Furthermore, the constraint of the circular containers introduces inevitable boundary effects. Future field-scale studies under fluctuating natural environmental conditions would be beneficial to further address scaling effects and support these macroscopic observations.

$$\frac{m_{\text{xanthan}}}{m_{\text{soil}}} = \frac{\theta_{\text{xanthan}}}{1 - \theta_{\text{xanthan}}} \tag{1}$$

$$m_w = \frac{m_0}{(1 + 0.01 w_0)} \times 0.01\,(w_1 - w_0) \tag{2}$$

where $m_{xanthan}$ is the quality of the xanthan gum (g), m_{soil} is the quality of the soil, mw is the quality of the water (g), m_0 is the amount of water required to add to the soil sample (g), w_0 is the air-dried moisture content (%), w_1 is the required moisture content for the soil sample (%), and $\theta_{xanthan}$ is the required xanthan gum content (%).

The weighing device and the shooting device together form the experimental monitoring device, as shown in Figure 4. The weighing device consists of a high-precision electronic scale. The sample is placed on a high-precision electronic scale and connected to a computer. To obtain a more accurate evaporation curve, the data is recorded every 2 h. The shooting device consists of a digital camera and a fill light. The camera is fixed directly above the sample, and the fill light is used to ensure that the photos taken are clear and free of shadows. The camera is set to take a photo every 2 h to record the changes in surface cracks of the sample. The experimental monitoring device, as a whole, is placed in a constant temperature and humidity chamber, with a set temperature of 25 °C and a relative humidity of 20%.

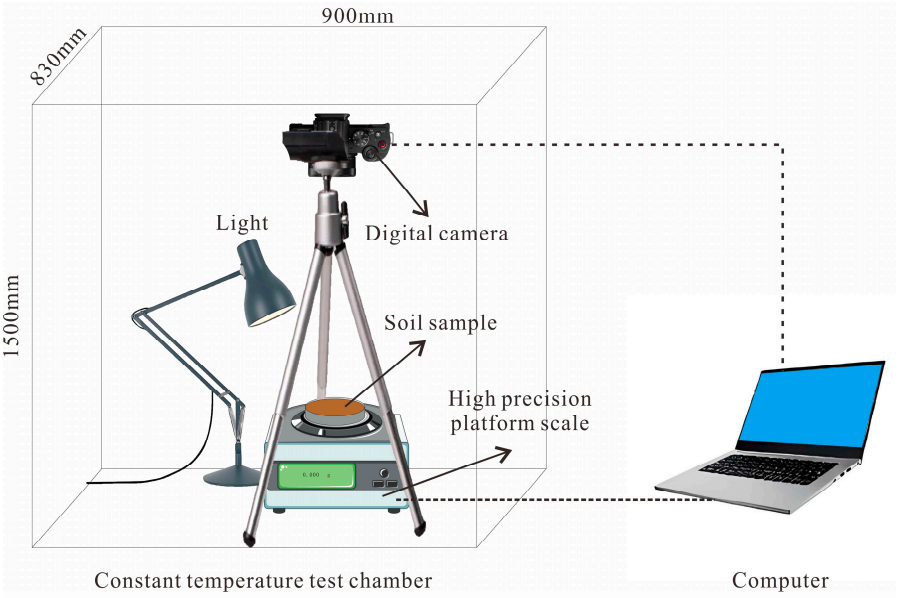


Figure 4. Experimental setup for soil desiccation tests, enabling continuous monitoring of evaporation dynamics and surface crack evolution.

2.3. Main Parameter Calculation and Image Processing

This study aims to determine the effect of xanthan gum on soil water retention by recording the changes in moisture content (w) and evaporation rate (E_v) during the evaporation process of soil samples. If the evaporation rate is low and the change in water content per unit time is small, it can be considered that the soil sample has good water retention performance; otherwise, the water retention performance is poor.

$$w = \frac{m - \Delta m}{m_d} \tag{3}$$

$$E_v = \frac{\Delta m}{t} \tag{4}$$

where m is the initial mass of water in the soil sample (g), $\triangle m$ is the change in sample weight (g), m_d is the weight of dry soil (g), and t is time (h).

A video data and fracture image analysis system based on a fixed camera calculates different fracture parameters, such as fracture fractal dimension (D) and fracture rate (C_R), through image segmentation, grayscale processing, binarization processing—which

was performed using Otsu's thresholding method to ensure objective and reproducible crack segmentation across all samples, minimizing user bias—and binary image denoising. The fractal dimension represents the similarity between the remaining structure and the original structure after a complete structure is damaged, and in this study, it represents the complexity of soil cracking. C_R utilizes the crack rate as the ratio of the area of soil cracking cracks to the total area of the soil.

$$C_R = S_{crack}/S_{soil} \tag{5}$$

$$D = \lim_{r \to 0} \frac{\log N(r)}{-\log r} \tag{6}$$

where S_{crack} is the projected two-dimensional crack surface area, S_{soil} is the projected two-dimensional surface area without cracks, and r is the square edge-length of the crack area; $N(r)$ is the number of squares; C_R is the calculated fractal dimension value.

The crack ratio and fractal dimension were quantitatively calculated based on high-resolution pixel-level binary image analysis. Because the segmentation and quantitative area calculations are highly sensitive to subtle morphological variations at the sub-millimeter scale, the resulting dynamic parameters and their relative differences are reported to two decimal places to maintain data fidelity and accurately reflect the pixel-based computational precision.

3. Results

3.1. Effect of Xanthan Gum Content on Moisture Evaporation from Soil

Figure 5 shows the curves of moisture content and evaporation rate for four samples with different xanthan gum contents (0.2%, 0.4%, 0.6%, 0.8%). According to the image, the evaporation process of the four samples can be divided into stage I (constant rate stage), stage II (deceleration rate stage), and stage III (residual evaporation stage). The moisture content shows a linear change in stage I, and when it reaches stage II, there is a nonlinear change in moisture content, at which point the evaporation rate also undergoes a sudden change. At the end of stage II, the moisture content gradually stabilizes.

Different levels of xanthan gum can alter the duration of each stage. The relative evaporation rates of soil samples with XG contents of 0.2%, 0.4%, 0.6%, and 0.8% in stage I were 2.27 g/h, 2.36 g/h, 2.46 g/h, and 2.46 g/h, respectively. The duration of stage I in the four groups of samples was 60 h, 58 h, 56 h, and 56 h, respectively. As the content of xanthan gum increases, the relative evaporation rate of stage I increases, and the duration decreases. However, when the content of xanthan gum is greater than 0.6%, the relative evaporation rate and duration of stage I reach consistency. When the moisture content decreases from 100% to around 31%, the evaporation rate of the soil sample shifts from stage I to stage II. When the moisture content of soil samples with an XG content of 0.2%, 0.4%, 0.6%, and 0.8% is 31.74%, 31.25%, 31.97%, and 31.04%, respectively, the evaporation rate begins to enter the deceleration stage. When the content of xanthan gum increased from 0.2% to 0.6%, the duration of stage II increased by 40%. When the content was 0.8%, the duration of stage II increased by 70%. The increase in xanthan gum content also advanced the start time of stage II, Compared to the soil sample with 0.2% XG content, the samples with 0.4%, 0.6%, and 0.8% XG content advanced by 2 h, 4 h, and 4 h, respectively. When the moisture content of soil samples with an XG content of 0.2%, 0.4%, 0.6%, and 0.8% decreases to 14.98%, 17.67%, 18.51%, and 13.52%, respectively, the soil sample enters stage III. The soil samples with an XG content of 0.8% entered stage III earlier than those with an XG content of 0.2%, 0.4%, and 0.6%. At the end of stage III, the final moisture contents corresponding to a xanthan gum content of 0.2%, 0.4%, 0.6%, and 0.8% were 4.05%, 5.21%, 9.71%, and

11.74%, respectively. The relative evaporation rates decreased by 83.26%, 83.05%, 87.8%, and 97.15%, respectively, compared to the rates in stage I.

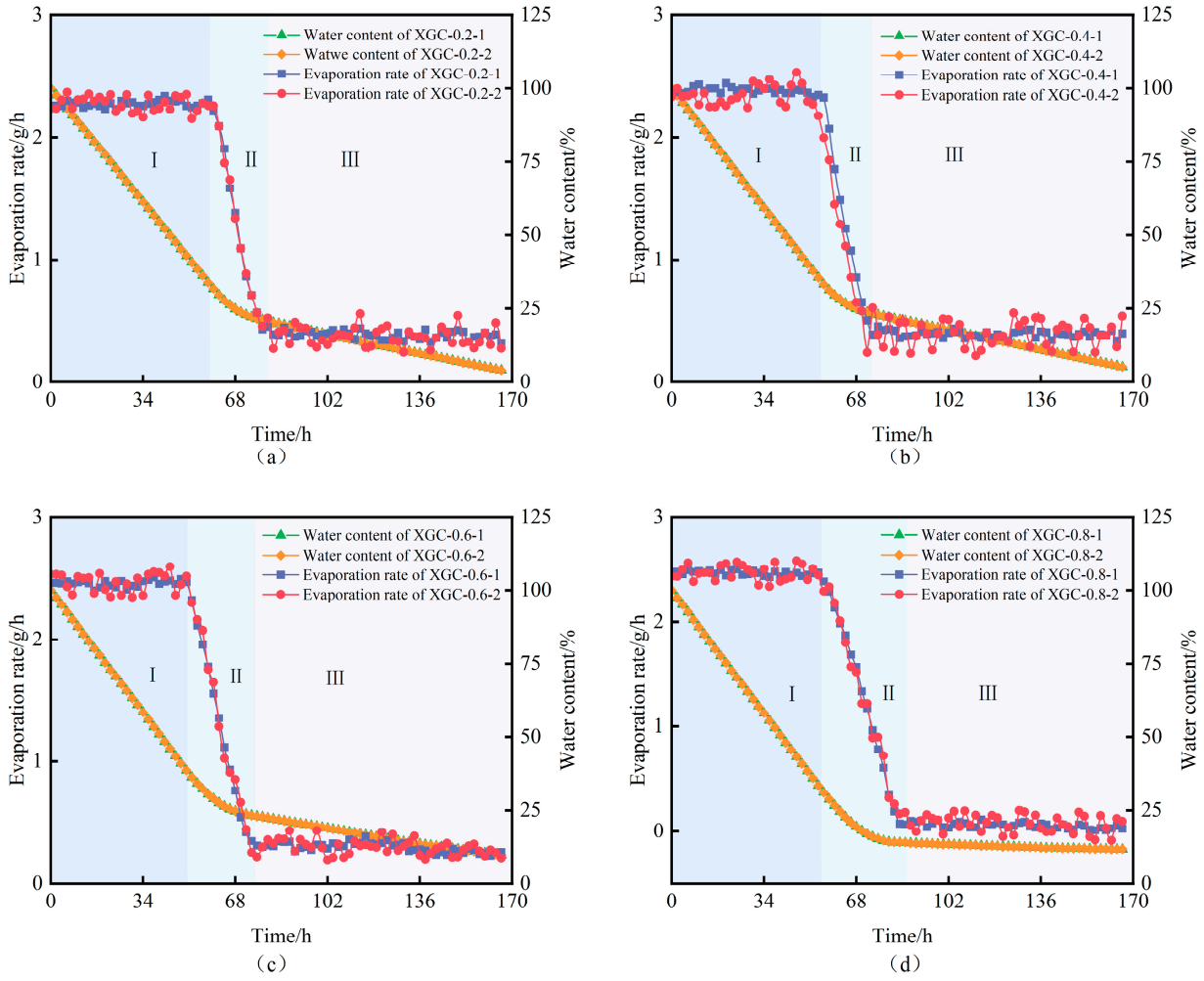


Figure 5. Time-history curve of evaporation rate and moisture content (all samples were prepared in identical containers (diameter 18 cm)): (**a**) contains 0.2% xanthan gum soil; (**b**) contains 0.4% xanthan gum soil; (**c**) contains 0.6% xanthan gum soil; (**d**) contains 0.8% xanthan gum soil.

3.2. Effect of Xanthan Gum Content on Soil Crack Development

The captured crack image is shown in Figure 6a. This article defines that at the beginning of the appearance of cracks, the first batch of cracks to appear are “trunks”, the cracks that branch from the trunks are “branches”, and the cracks that split from the branches are “twigs”. It should be explicitly clarified that the parameter-free Otsu algorithm, the descriptive “trunk–branch–twig” terminology, and the kinetic calculations are employed as macroscopic phenomenological tools. They serve as first-order approximations to quantify surface morphological evolution rather than as rigorous micro-fracture mechanics models.

According to the image, the cracking moisture content of the four groups of samples is around 31%. In the early stage of cracking, the soil containing 0.2% XG shows obvious trunks which run through the entire soil sample. The trunks of soil containing 0.4% XG mainly appears at the edges of the soil sample, while the soil with 0.6% XG only shows some subtle and shallow cracks at the edges. However, the cracks in the soil with 0.8% XG are not only shallow but are also only 2 cm long. During the cracking period, in terms of the overall development process of the sample cracks, the new cracks generated during the crack development process are mainly generated and developed at the trunk location. The

rapid expansion of cracks causes the trunk to become longer and deeper, while inducing the development of subsequent cracks and cracking in all directions, forming a crack grid.

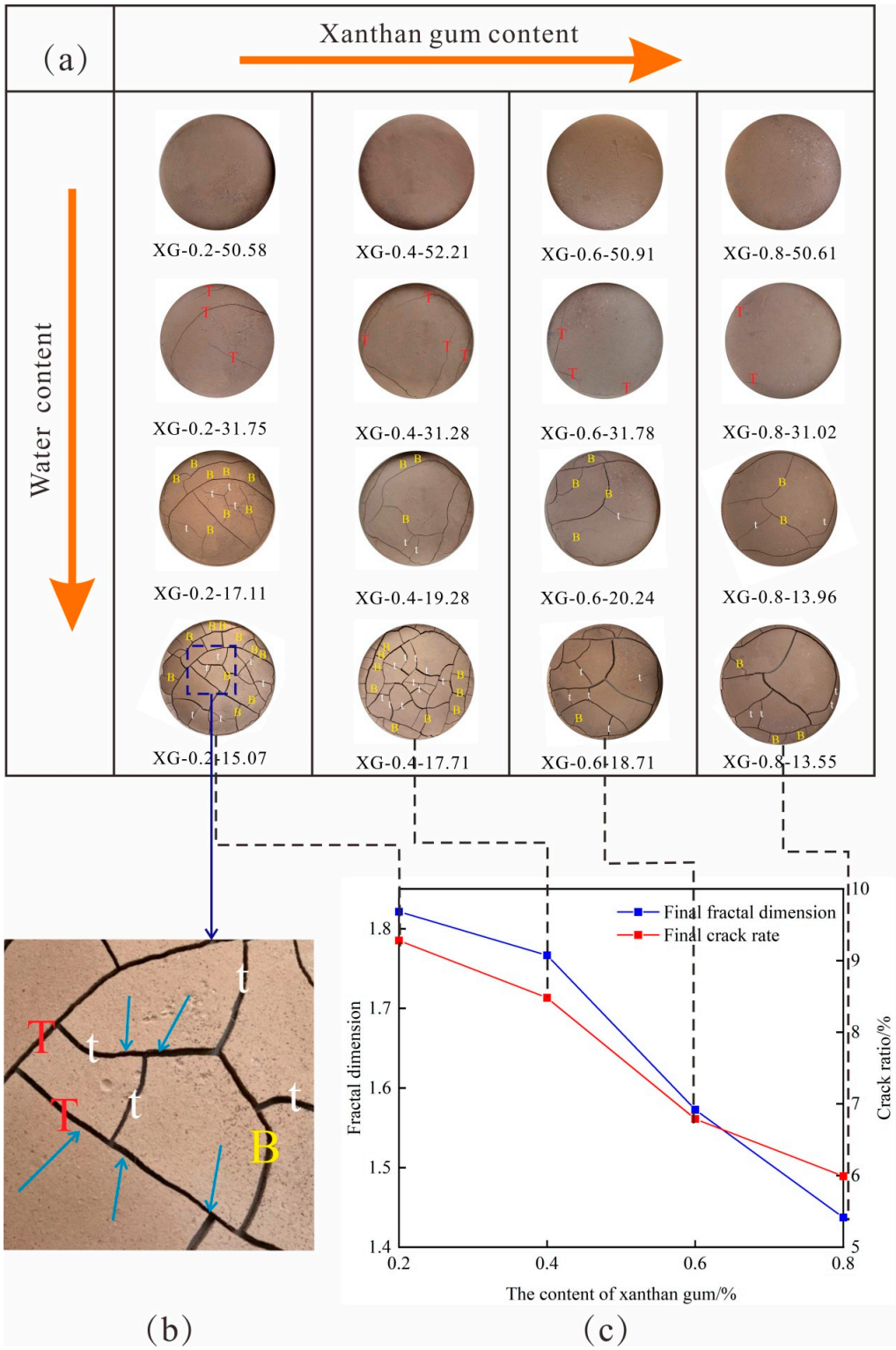


Figure 6. (**a**) Fracture image analysis; (**b**) fracture development map; (**c**) final fracture rate and final fractal dimension.

As shown in Figure 6b, the development of branches is mostly perpendicular to the trunk, dividing the sample into multiple polygons, but mainly quadrilaterals. In the later stage of cracking, the cracks in the soil sample with a content of 0.2% XG are mainly

branches, and as the XG content increases, twigs begins to dominate. At this stage, the pattern of cracking no longer changes, but the moisture content is still decreasing. There is a clear difference in the moisture content at the end of cracking, with soil samples with XG contents of 0.2%, 0.4%, 0.6%, and 0.8% ending in cracking at 15.07%, 17.71%, 18.71%, and 13.55%, respectively. The measured moisture content varies at the time of shooting. After the cracking is completed, it can be intuitively observed from the image that the soil sample with an XG content of 0.8% shows the least number cracks, and twigs are the main type of crack. The soil samples with XG contents of 0.4% and 0.6% exhibit more cracks, followed by the soil sample with an XG content of 0.2% with the greatest number of cracks, and the proportion of cracks of the trunk and branch type in this group is the highest. This phenomenon can be verified by the (c) graph in Figure 6, showing the final fracture rate and final fracture dimensions. The final crack rate decreases linearly with the content of xanthan gum. The final crack rates of soil samples with an XG content of 0.4%, 0.6%, and 0.8% decreased by 9.43%, 36.66%, and 54.91%, respectively, compared to the results for the soil samples with an XG content of 0.2%. Compared with the complexity of the number and shape of cracks in soil samples with an XG content of 0.2% and 0.4%, the complexity of soil samples with an XG content of 0.6% and 0.8% has been significantly improved. This phenomenon can be confirmed by the fractal dimensions. The fractal dimension of soil samples with an 0.4% XG content decreased by only 3.02% compared to the rate for soil samples with a 0.2% XG content, while the fractal dimensions of soil samples with a 0.6% and 0.8% XG content decreased by 15.72% and 26.62%, respectively.

3.3. Kinetic Analysis of Crack Development

As shown in Figures 7 and 8, the cracking time of the four groups of samples is approximately 58 h, and prior to that, the samples did not crack. The fractal dimension and fracture rate both show a trend of first increasing and then stabilizing with the decrease in moisture content.

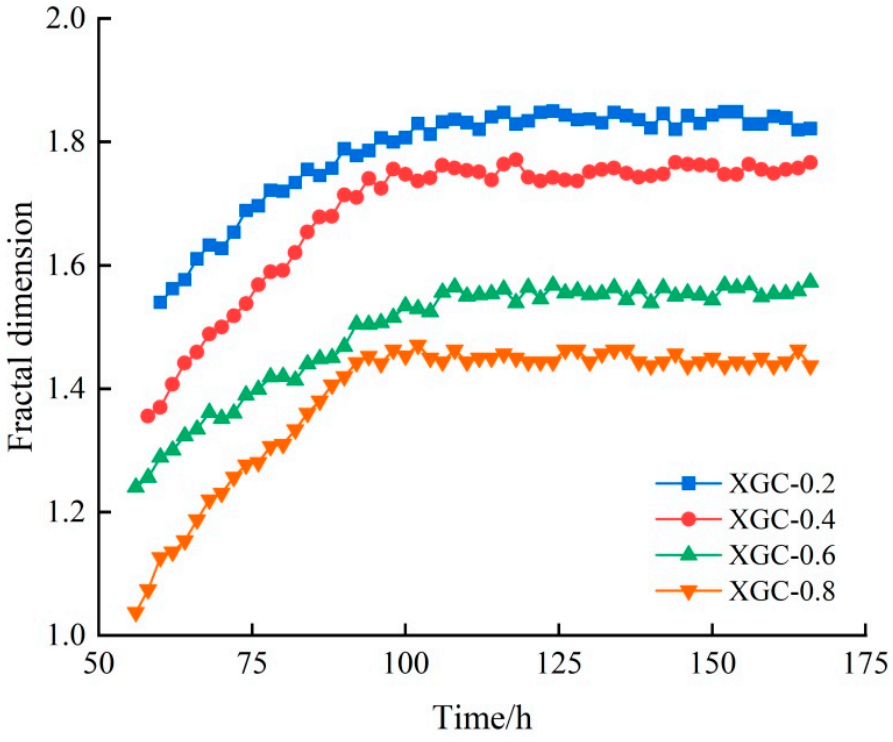


Figure 7. Fractal dimensions for different XG contents.

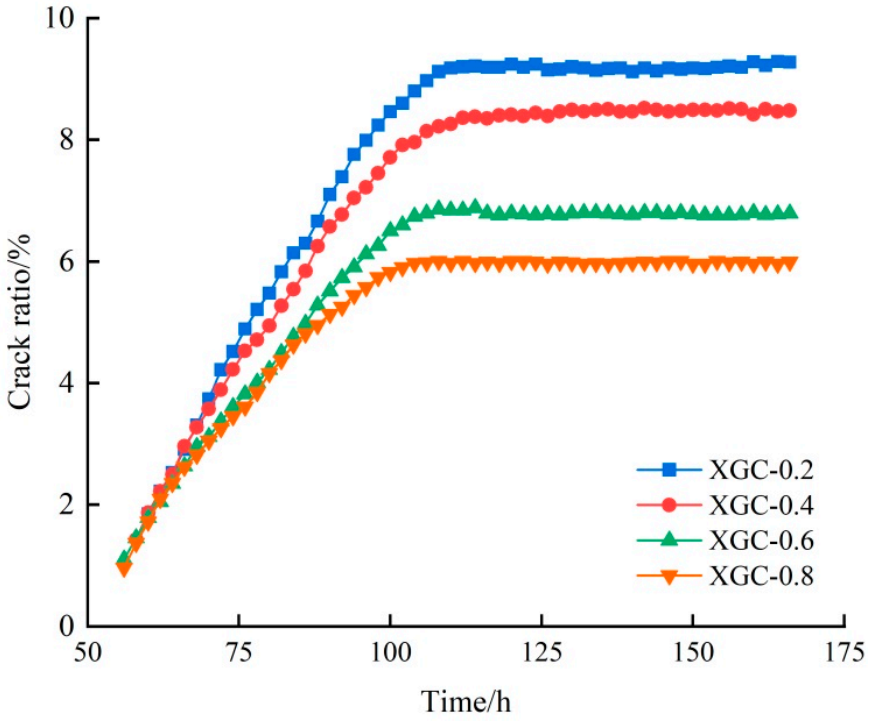


Figure 8. Fracture rate of soil with different XG contents.

The fractal dimension and fracture rate show a decreasing trend with the increase in xanthan gum content in the soil sample. At the beginning of cracking, there were very few cracks in the four specimens, and the difference in crack rate was not significant. As the moisture content gradually decreases, cracks begin to develop, and there is a clear difference in crack rate due to the different XG contents in the soil sample. At the beginning of soil cracking, the fractal dimension of the sample with an XG content of 0.2% was 11.99%, 19.48%, and 32.64% higher than that of the soil samples with XG contents of 0.4%, 0.6%, and 0.8%, respectively. When the cracking tends to stabilize, the fractal dimension and crack rate also tend to stabilize. At this point, the sample with an XG content of 0.2% has an average fractal dimension of 1.84 and an average fracture rate of 9.19%. The fractal dimensions of soil samples with an XG content of 0.4%, 0.6%, and 0.8% decreased by 4.89%, 15.76%, and 21.2%, respectively, compared to the results for sample with an XG content of 0.2%. The average crack rates decreased by 13.82%, 26.12%, and 35.15%, respectively. This reflects that the cracking situation of the soil with a 0.2% and 0.4% content is similar, with multiple and complex cracks, while the soil with a 0.6% and 0.8% content has fewer and simpler cracks compared to those in the first two samples. According to Figure 6a, it can be intuitively observed that there is the most significant difference between the soil with a xanthan gum content of 0.4% and the soil with a content of 0.6%, so there is a large change in the fractal dimension during stabilization.

To further quantify the dynamic process, we calculated the average crack development rate (v_{crack}) and the average fractal dimension change rate (v_{FD}) from crack initiation (58 h) to stabilization using the data presented in Figures 7 and 8.

The average crack development rate was defined as

$$v_{crack} = \frac{CR_{final} - CR_{init}}{t_{stable} - t_{init}} \quad (7)$$

where CR_{final} = final crack ratio at stabilization (%), CR_{init} = initial crack ratio at crack initiation (taken as 0%), t_{stable} = time at which the crack ratio stabilizes (h), and t_{init} = crack initiation time (58 h in this study).

Similarly, the average fractal dimension change rate was calculated as

$$v_{FD} = \frac{FD_{final} - FD_{init}}{t_{stable,FD} - t_{init}} \quad (8)$$

where FD_{final} = fractal dimension at stabilization (dimensionless), FD_{init} = fractal dimension at crack initiation (taken as 1.00, representing a crack-free state), $t_{stable,FD}$ = time at which the crack ratio stabilizes (h), and t_{init} = crack initiation time (58 h).

Based on these definitions, the calculated kinetic parameters for different xanthan gum contents are summarized in Table 2.

Table 2. Kinetic parameters of crack development for different xanthan gum (XG) contents.

XGC (%)	$t_{stable,FD}$ (h)	Final Crack Ratio (%)	v_{crack} (%/h)	$t_{stable,FD}$ (h)	FD_{final}	v_{FD} (h^{-1})
0.2	112	9.20	0.170	106	1.83	0.017
0.4	110	8.36	0.161	105	1.76	0.016
0.6	104	6.80	0.148	106	1.55	0.011
0.8	104	5.96	0.130	94	1.45	0.013

The results are summarized in Table 2. For the 0.2% XG sample, v_{crack} = 0.170%/h, and v_{FD} = 0.017 h^{-1}. As XG content increased to 0.8%, v_{crack} decreased to 0.1296%/h (a reduction of 24.0%), and v_{FD} decreased to 0.01250 h^{-1} (a reduction of 27.7%). These kinetic calculations quantitatively confirm that xanthan gum effectively slows down crack propagation dynamics, not only reducing the final crack ratio and fractal dimension but also significantly decreasing the rate of crack propagation. The reduction in crack development rate is particularly pronounced between 0.2% and 0.6% XG, after which further increases in XG content yields diminishing returns.

4. Discussion

The generation and development of soil cracks largely depend on soil evaporation. The larger soil environment humidity gradient affects the changes and distribution characteristics of soil moisture, as well as the hydraulic behavior of soil [18]. This large soil environment humidity gradient exacerbates the accumulation of tensile stress within the entire soil sample. Once the accumulation of tensile stress exceeds the tensile strength of the soil, dry cracking will quickly occur in the soil. The cracks in the cracked soil will continue to evolve and develop, forming a stable trend of cracks [35]. It should be noted that the mechanistic interpretations discussed herein are inferred based on our macroscopic quantitative observations, coupled with the established physicochemical properties of the high-purity commercial xanthan gum.

The development of cracks is mainly due to the shrinkage of soil volume under evaporation. When XG is added to the soil, the pores in the soil contain not only water but also XG particles. In the early stage of evaporation, because the soil is completely saturated, the rate of soil evaporation is equal to the loss of pore water. To explicitly resolve the apparent contradiction in which the stage I evaporation rate slightly increases with higher XG content, while overall water retention is improved, it should be noted that in the initial fully saturated state (stage I), the highly hydrophilic functional groups (e.g., carboxyl and hydroxyl) of xanthan gum actively bind and transport moisture to the evaporative surface, slightly elevating the initial evaporation rate. However, as desiccation progresses into stages II and III, the biopolymer rapidly undergoes volumetric shrinkage and forms the aforementioned dense hydrogel network, interrupting capillary continuity and fundamentally inhibiting subsequent moisture loss.

As the evaporation process continues, in addition to water and XG, air also enters the soil, leading to soil unsaturation and a significant increase in suction. The surface structure of dry shrinkage cracks is mainly composed of interwoven crack networks and "cut" blocks, and the fractal dimension and crack rate are quantitative descriptions of dry shrinkage cracks. The fractal dimension is an important parameter for quantitatively characterizing the complexity and roughness of soil shrinkage cracks. The larger the fractal dimension, the more complex and rougher the cracks and vice versa. Crack rate is a quantitative description of the width and development degree of soil shrinkage cracks. As the moisture content continued to decrease, the slope of the moisture content curve of the soil with 0.2% XG changed after 66 h, while the soil with 0.4% XG and 0.6% XG shortened the time by 4 h and 6 h compared to the rate for the soil with 0.2% XG. Xanthan gum delays the evaporation rate of water by filling pores [36,37]. With the increase in xanthan gum content, the encapsulation effect between xanthan gum and soil particles is enhanced. Due to the ability of biopolymers to absorb water (pure xanthan gum can hold approximately 25 times the weight of water), soil particles and xanthan gum that are located close together are interconnected. When biopolymers adsorb more water, they form aggregates [38], leading to an increase in the soil's water retention capacity. The slope change of soil moisture content in soil with 0.8% XG content was delayed by 14 h compared to the rate for soil with a 0.6% XG content. This is because high concentrations of xanthan gum can cause soil pore blockage, leading to a decrease in soil evaporation rate [23].

The kinetic calculations reveal that increasing the xanthan gum (XG) content from 0.2% to 0.8% reduces the average crack development rate (v_{crack}) by 24.0% and the fractal dimension change rate (v_{FD}) by 27.7%. These results quantitatively demonstrate that XG not only suppresses final crack severity but also slows down the crack propagation process itself.

The retardation effect likely arises from the polymeric network formed by XG, which binds soil particles and retains water during dehydration. This network shrinks gradually, buffering tensile stresses that drive crack growth. The diminishing returns beyond 0.6% XG suggests an optimal dosage around 0.6–0.8% for practical applications such as landfill covers or slope protection. Future work should couple crack kinetics with evaporation rates to establish a direct cause–effect relationship.

The addition of xanthan gum reduces the pores of the soil, lowers its capillary conductivity, and thus improves its water retention capacity [21]. With the decrease in water content, the xanthan gum solution changes into a gelled state when combined with the soil particles. Compared with the liquid state, gel state has higher viscosity and elasticity, which can significantly enhance the tensile strength between particles, the cohesion, and the friction of the soil [22].

As shown in Figure 9, the final moisture content of the four groups of samples was positively correlated with the xanthan gum (XG) content. Error bars indicate standard deviation (SD, n = 3). A one-way ANOVA showed that XG content had a statistically significant effect on the residual moisture content ($F(3, 8) = 2366.2$, $p < 0.0001$).

For direct comparison, the relationship between the four types of fracture rates and the residual moisture content is plotted in Figure 10. The increase in xanthan gum content significantly restricts the propagation of crack networks.

During the drying and dehydration process, xanthan gum aggregates form a high molecular weight coating, reducing the rate of water evaporation in the soil [39,40]. With the increase in XG content, the soil fracture rate is effectively reduced. For soils with low XG content, due to the limited presence of xanthan gum aggregates between pores and weak bonding between particles, the matrix suction between soil particles dominates, and the role of xanthan gum aggregates is relatively small, making it easy for dry cracks to

develop rapidly. With the increase in XG content, the aggregates in the soil pores increase, and the binding between xanthan gum aggregates and particles strengthens, forming a polymer grid to share the internal matrix suction and reduce the formation of cracks [41].

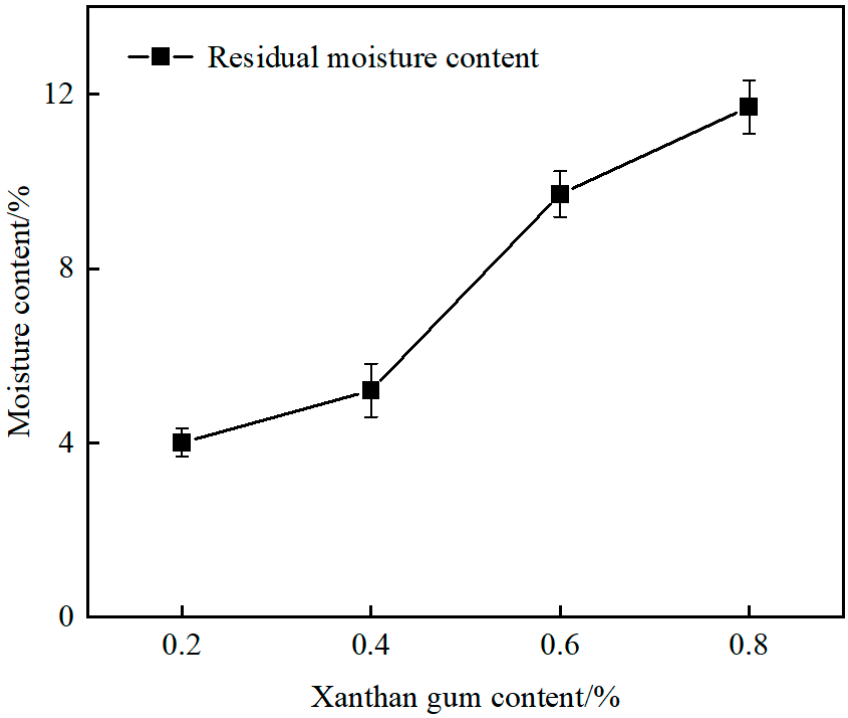


Figure 9. Residual moisture content variation curve.

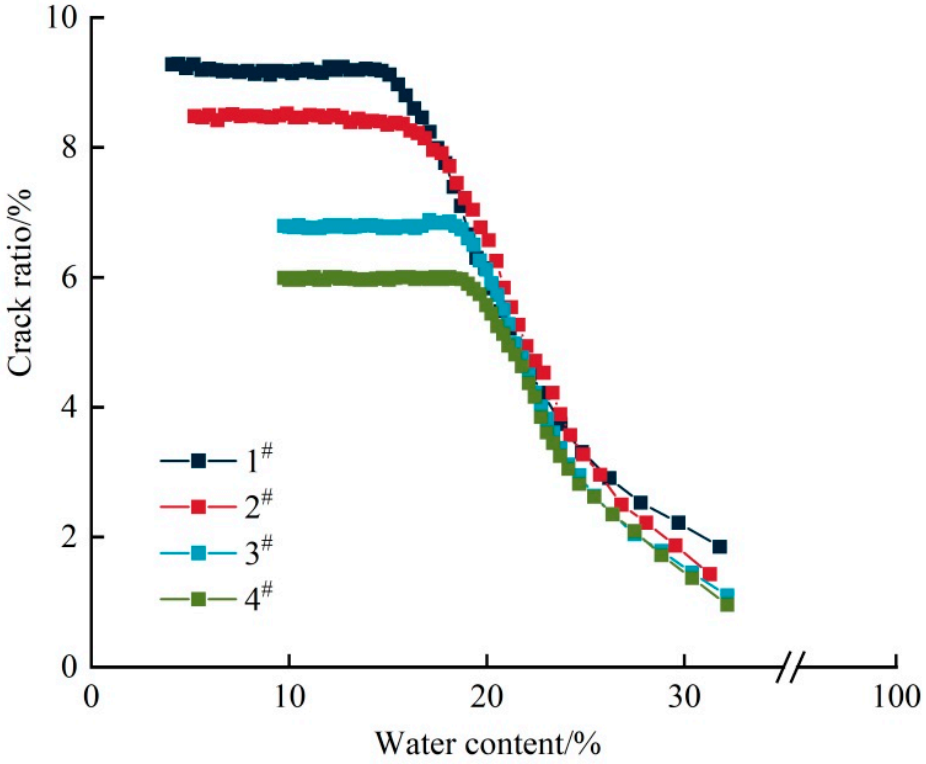


Figure 10. Relationship between fracture rate and moisture content.

Experiments have shown that the presence of xanthan gum improves soil water retention and crack resistance by influencing the internal forces and tight particle arrangement of the soil, forming biological aggregates that encapsulate xanthan gum, soil particles,

and water. Due to the saturated state of the soil sample, xanthan gum contains a large number of carboxyl (-COOH) and hydroxyl (-OH) groups, which can form stable polymer mesh structures with soil particles through hydrogen bonding and electrostatic bonding. Xanthan gum in the gel state uses its cementation ability to form a "bridge" structure with the surrounding soil particles, thus enhancing the tensile strength of the soil [42]. As shown in Figure 11, the presence of xanthan gum increases the coupling force between soil particles [43]. The greater the coupling force between soil particles, the higher the tensile strength and the stronger the crack resistance. During the drying process, the presence of xanthan gum significantly reduces the number of soil pores. The reduction of pore volume leads to a decrease in capillary pressure, thereby reducing the impact of capillary pressure and separation pressure on overall drying shrinkage. The soil improved by xanthan gum shortens with dehydration, and the polymer mesh shrinks with drying [41]. However, due to the bridging structure between the polymer grid and the surrounding soil, the risk of soil cracking is significantly reduced. During the drying and dehydration process, the O–H bond of the polymer becomes shorter, and the interaction force between aggregates decreases, resulting in cracks in the soil sample.

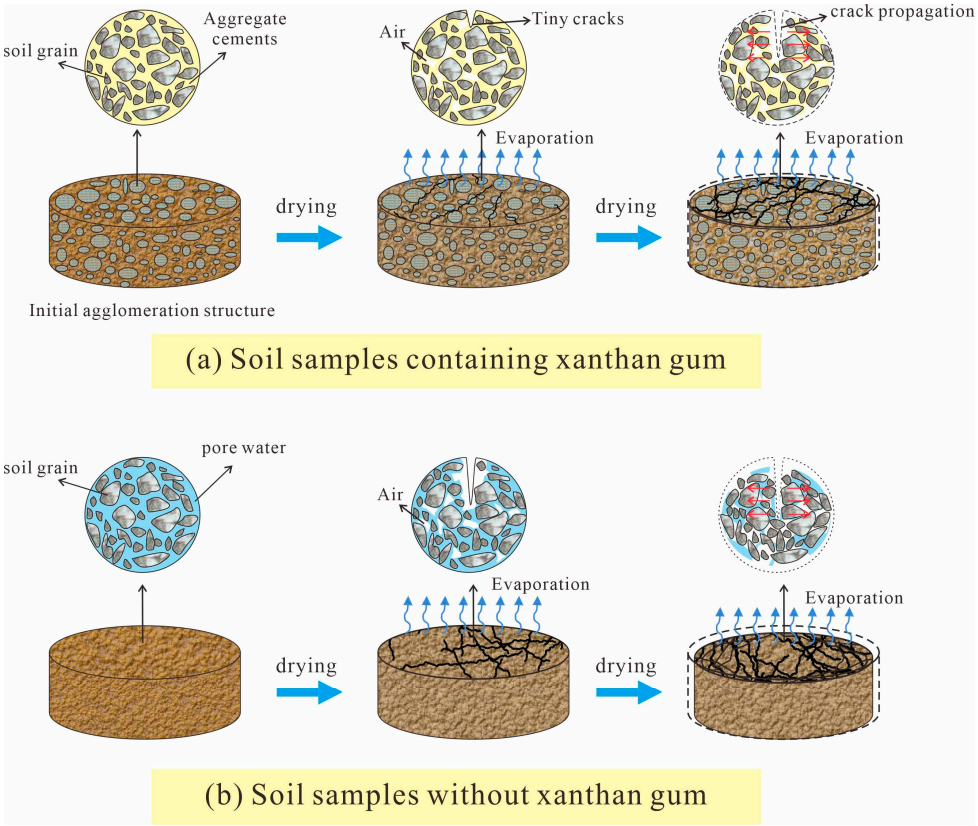


Figure 11. Soil mechanism diagram during the drying process.

5. Conclusions

This study conducted soil drying and cracking tests to investigate the effects of different xanthan gum contents on soil crack resistance and water retention. The results show that xanthan gum alters the soil evaporation process, which can be divided into three stages: the constant rate stage, the deceleration rate stage, and the residual stage. Adding xanthan gum to soil reduces soil cracking. The crack rate and fractal dimension of soil decrease with increasing xanthan gum content, while the duration of the deceleration stage is prolonged, and the final residual water content increases markedly, with a maximum increase of 192.5%, suggesting a possible improvement in water retention.

The hypothesized mechanism by which xanthan gum affects soil cracking involves the change in soil pore volume and the water absorption of xanthan gum. Xanthan gum becomes a hydrogel after absorbing water, which is inferred to occupy the pore space of the soil and reduce the capillary conductivity of the soil. Due to its strong water absorption capacity, xanthan gum enhances the soil's water retention during the drying process. The macroscopically observed ability to resist drought is more significant in soils with high xanthan gum content than in soils with low xanthan gum content. In addition, compared with the results for untreated soil, in the soil treated with 0.2% xanthan gum, the crack rate decreases by up to 54.91%, and the crack morphology gradually changes from dominant trunk structures to finer branch and twig patterns.

When soils with different xanthan gum contents transition from the constant rate stage to the deceleration rate stage, their moisture content is approximately 31%. The sample with better crack resistance is soil with a xanthan gum content of 0.6%, as high concentrations of xanthan gum are limited by soil structure. Further increasing the xanthan gum content to 0.8% does not result in a proportional improvement, which may be attributed to excessive pore filling and structural constraints.

When the binding between xanthan gum aggregates and particles is relatively weak, matrix suction dominates during the drying process. But when the content of xanthan gum increases, it is inferred that a polymer grid is formed between the aggregates and the soil particles, which hypothetically shares some of the matrix suction and significantly enhances the tensile strength between particles and the cohesion of the soil. Therefore, the addition of xanthan gum enhances the soil's water retention and crack resistance. It can be used as an environmentally friendly and economical soil amendment. This study was conducted under laboratory conditions, with a limited range of environmental settings and soil characterization. Therefore, the findings should be generalized with caution. Future field-scale studies with more comprehensive soil characterization are needed to further validate the conclusions.

Author Contributions: B.Y.: data curation; writing—review and editing. Y.Y.: writing—review and editing; writing—original draft. All authors have read and agreed to the published version of the manuscript.

Funding: This study is funded by the Key Scientific Research Projects of Colleges and Universities in Henan Province (25B410001, 25B570003).

Data Availability Statement: The original contributions presented in this study are included in the article. Further inquiries can be directed to the corresponding author.

Conflicts of Interest: The authors declare that they have no known competing financial interests or personal relationships that could have appeared to influence the work reported in this paper.

References

1. Costa, S.; Kodikara, J. Shrinkage development during soil desiccation. In *Unsaturated Soils, Two Volume Set: Experimental Studies in Unsaturated Soils and Expansive Soils (Vol. 1) & Theoretical and Numerical Advances in Unsaturated Soil Mechanics (Vol. 2)*; CRC PRESS: Boca Raton, FL, USA, 2009; p. 433.
2. Zhu, H.; Fu, Z.; Wen, S.; Chen, J.; Xiao, Y. Evolution of LWAC–OC interfacial properties during sulfate dry–wet cycles: Bonding strength and micro–properties. *J. Build. Eng.* **2024**, *92*, 109780. [CrossRef]
3. Sun, M.; Li, X.; Zhang, D.; Lin, B.; Hao, J.; Liu, J. Effect of basalt fiber and carbon fiber on the evolution of water evaporation and cracking characteristics of silt soil. *Can. J. Soil Sci.* **2024**, *104*, 204–215. [CrossRef]
4. Cheng, Q.; Tang, C.S.; Xu, D.; Zeng, H.; Shi, B. Water infiltration in a cracked soil considering effect of drying-wetting cycles. *J. Hydrol.* **2021**, *593*, 125640. [CrossRef]
5. Masoudi, M.; Nooraiepour, M.; Deng, H.; Hellevang, H. Mineral Precipitation and Geometry Alteration in Porous Structures: How to Upscale Variations in Permeability–Porosity Relationship? *Energy Fuels* **2024**, *38*, 9988–10001. [CrossRef]

6. Karan, S.; Jensen, K.H.; Sonnenborg, T.O. Numerical prediction uncertainty and data worth analysis of solute transport in an agricultural clay till setting with preferential flow. *Water Resour. Res.* **2024**, *60*, e2023WR036557. [CrossRef]
7. Feng, L.; Zhang, M.; Liu, H.; Zhang, B.; Du, Z.; Sun, P.; Bi, J.; Wang, L.; Gu, T. The general patterns of water flow in loess slope system and implications for slope geological security. *Sci. Total Environ.* **2024**, *945*, 174041. [CrossRef]
8. Tang, C.; Shi, B.; Liu, C.; Zhao, L.; Wang, B. Influencing factors of geometrical structure of surface shrinkage cracks in clayey soils. *Eng. Geol.* **2008**, *101*, 204–217. [CrossRef]
9. Shaker, A.A.; Dafalla, M.; Al-Mahbashi, A.M.; Al-Shamrani, M.A. Effect of Drying and Wetting Cycles on the Surface Cracking and Hydro-Mechanical Behavior of Expansive Clays. *Buildings* **2024**, *14*, 1908. [CrossRef]
10. Amenuvor, A.C.; Li, G.; Wu, J.; Hou, Y.; Chen, W.; Charkley, F.N. Crack development in a physical model of undisturbed expansive soil slope and core sample under wet-dry cycles. *Eur. J. Environ. Civ. Eng.* **2024**, *28*, 822–843. [CrossRef]
11. Whiteley, G.M.; Dexter, A.R. The behaviour of roots encountering cracks in soil: I. Experimental methods and results. *Plant Soil* **1984**, *77*, 141–149. [CrossRef]
12. Azim, R.; Wang, Q.; Mak-Mensah, E.; Zhou, X.; Zhang, D.; Zhao, X.; Qi, W.; Zhu, J.; Ma, W.; Sadiq, M.; et al. Soil desiccation in the context of vegetation restoration: A scientometric analysis. *Land Degrad. Dev.* **2024**, *35*, 4364–4378. [CrossRef]
13. Ettehadi, A.; Chuprin, M.; Mokhtari, M.; Anderson, R.C. Laboratory testing of desiccation crack growth in terrestrial Martian analog environments using digital image correlation. *Planet. Space Sci.* **2024**, *248*, 105933. [CrossRef]
14. Saliba, J.; Kouta, N.; Saiyouri, N. Effect of wetting/drying cycles on the durability of flax fibers reinforced earth concrete. *Constr. Build. Mater.* **2024**, *445*, 137924. [CrossRef]
15. Song, W.K.; Cui, Y.J.; Tang, A.M.; Ding, W.Q.; Wang, Q. Experimental study on water evaporation from compacted clay using environmental chamber. *Can. Geotech. J.* **2016**, *53*, 1293–1304. [CrossRef]
16. Cuadrado, A.; Najdi, A.; Ledesma, A.; Olivella, S.; Prat, P.C. THM analysis of a soil drying test in an environmental chamber: The role of boundary conditions. *Comput. Geotech.* **2022**, *141*, 104495. [CrossRef]
17. Hallett, P.D.; Newson, T.A. Describing soil crack formation using elastic–plastic fracture mechanics. *Eur. J. Soil Sci.* **2005**, *56*, 31–38. [CrossRef]
18. Zeng, H.; Tang, C.S.; Zhu, C.; Vahedifard, F.; Cheng, Q.; Shi, B. Desiccation cracking of soil subjected to different environmental relative humidity conditions. *Eng. Geol.* **2022**, *297*, 106536. [CrossRef]
19. Getahun, M.J.; Kassie, B.B.; Alemu, T.S. Recent advances in biopolymer synthesis, properties, & commercial applications: A review. *Process Biochem.* **2024**, *145*, 261–287.
20. Saha, A.; Sreedeep, S.; Manna, U. Role of Biopolymers and Their Composites in Sustainable Agriculture: Recent Developments and Future Perspectives. In *Applications of Biopolymers in Science, Biotechnology, and Engineering*; John Wiley & Sons: Hoboken, NJ, USA, 2024; pp. 57–87.
21. Zhang, J.; Liu, J.; Cheng, Y.; Jiang, T.; Saberian, M. Water-retention behaviour and microscopic analysis of two biopolymer-improved sandy soils. *Constr. Build. Mater.* **2023**, *403*, 133202. [CrossRef]
22. Chen, C.; Wu, L.; Perdjon, M.; Huang, X.; Peng, Y. The drying effect on xanthan gum biopolymer treated sandy soil shear strength. *Constr. Build. Mater.* **2019**, *197*, 271–279. [CrossRef]
23. Chang, I.; Lee, M.; Tran, A.T.P.; Lee, S.; Kwon, Y.M.; Im, J.; Cho, G.C. Review on biopolymer-based soil treatment (BPST) technology in geotechnical engineering practices. *Transp. Geotech.* **2020**, *24*, 100385. [CrossRef]
24. Schlüter, S.; Sammartino, S.; Koestel, J. Exploring the relationship between soil structure and soil functions via pore-scale imaging. *Geoderma* **2020**, *370*, 114370. [CrossRef]
25. Pourakbar, S.; Huat, B.K. A review of alternatives traditional cementitious binders for engineering improvement of soils. *Int. J. Geotech. Eng.* **2017**, *11*, 206–216. [CrossRef]
26. Chang, I.; Cho, G.C. Geotechnical behavior of a beta-1, 3/1, 6-glucan biopolymer-treated residual soil. *Geomech. Eng.* **2014**, *7*, 633–647. [CrossRef]
27. Orts, W.J.; Sojka, R.E.; Glenn, G.M. Biopolymer additives to reduce erosion-induced soil losses during irrigation. *Ind. Crops Prod.* **2000**, *11*, 19–29. [CrossRef]
28. Wang, N.; Wang, B.; Wan, Y.; Gao, B.; Rajput, V.D. Alginate-based composites as novel soil conditioners for sustainable applications in agriculture: A critical review. *J. Environ. Manag.* **2023**, *348*, 119133. [CrossRef]
29. Soldo, A.; Miletić, M.; Auad, M.L. Biopolymers as a sustainable solution for the enhancement of soil mechanical properties. *Sci. Rep.* **2020**, *10*, 267. [CrossRef]
30. Ni, J.; Li, S.S.; Ma, L.; Geng, X.Y. Performance of soils enhanced with eco-friendly biopolymers in unconfined compression strength tests and fatigue loading tests. *Constr. Build. Mater.* **2020**, *263*, 120039. [CrossRef]
31. Wu, Y.; Ding, W.; He, Q. The gelation properties of tara gum blended with κ-carrageenan or xanthan. *Food Hydrocoll.* **2018**, *77*, 764–771. [CrossRef]
32. Al-Awad, K. The Effect of Biological Exudates on the Mechanical Properties of Granular Soil. Doctoral Dissertation, Cardiff University, Cardiff, UK, 2018.

33. Barrere, G.C.; Barber, C.E.; Daniels, M.J. Molecular cloning of genes involved in the production of the extracellular polysaccharide xanthan by Xanthomonas campestris pv. campestris. *Int. J. Biol. Macromol.* **1986**, *8*, 372–374. [CrossRef]
34. Pydi, R.; Yadu, L.; Chouksey, S.K. Evaluation of Xanthan and Guar Gum for Stabilising Soil in Terms of Strength Parameters-A Review. *Indian Geotech. J.* **2024**, *54*, 1621–1643. [CrossRef]
35. Murray, I.; Tarantino, A. Mechanisms of failure in saturated and unsaturated clayey geomaterials subjected to (total) tensile stress. *Géotechnique* **2019**, *69*, 701–712. [CrossRef]
36. Cabalar, A.F.; Awraheem, M.H.; Khalaf, M.M. Geotechnical properties of a low-plasticity clay with biopolymer. *J. Mater. Civ. Eng.* **2018**, *30*, 04018170. [CrossRef]
37. Arabani, M.; Shalchian, M.M.; Baghbani, A. A state-of-the-art review on interactive mechanisms and multi-scale application of biopolymers (BPs) in geo-improvement and vegetation growth. *J. Environ. Manag.* **2024**, *358*, 120905. [CrossRef] [PubMed]
38. Zhou, C.; So, P.S.; Chen, X.W. A water retention model considering biopolymer-soil interactions. *J. Hydrol.* **2020**, *586*, 124874. [CrossRef]
39. Bouazza, A.; Gates, W.P.; Ranjith, P.G. Hydraulic conductivity of biopolymer-treated silty sand. *Géotechnique* **2009**, *59*, 71–72. [CrossRef]
40. Shashirekha, V.; Sowmiya, V.; Malleswari, R.B.; Seshadri, S. Conserving soil microbial population and sustainable agricultural practices—Polymers in aid of safe delivery, protection, population enhancement, and maintenance. In *Beneficial Microbes for Sustainable Agriculture Under Stress Conditions*; Academic Press: Cambridge, MA, USA, 2024; pp. 313–358.
41. Kudo, K.; Ishida, J.; Syuu, G.; Sekine, Y.; Ikeda-Fukazawa, T. Structural changes of water in poly (vinyl alcohol) hydrogel during dehydration. *J. Chem. Phys.* **2014**, *140*, 4. [CrossRef]
42. Chen, Z.; Liu, J.; Wang, Y.; Qi, C.; Ma, X.; Che, W.; Ma, K. Wetting–drying effects on the mechanical performance of xanthan gum biopolymer-stabilized soil. *Environ. Earth Sci.* **2024**, *83*, 197. [CrossRef]
43. Chang, I.; Im, J.; Prasidhi, A.K.; Cho, G.C. Effects of Xanthan gum biopolymer on soil strengthening. *Constr. Build. Mater.* **2015**, *74*, 65–72. [CrossRef]

Disclaimer/Publisher's Note: The statements, opinions and data contained in all publications are solely those of the individual author(s) and contributor(s) and not of MDPI and/or the editor(s). MDPI and/or the editor(s) disclaim responsibility for any injury to people or property resulting from any ideas, methods, instructions or products referred to in the content.